## Supplementary Information for "Plasmonic nanofocusing spectral interferometry"

Martin Esmann<sup>1,2,‡</sup>, Abbas Chimeh<sup>1,‡</sup>, Anke Korte<sup>1</sup>, Jin-Hui Zhong<sup>1</sup>, Sven Stephan<sup>1</sup>, Julia Witt<sup>3</sup>,

Gunther Wittstock<sup>3</sup>, Nahid Talebi<sup>4,5</sup>, Christoph Lienau<sup>1,6</sup>\*

<sup>1</sup> Institute of Physics and Center of Interface Science, Carl von Ossietzky University, 26111 Oldenburg, Germany

<sup>2</sup> Centre for Nanoscience and Nanotechnology (C2N), CNRS, Université Paris-Sud, Université Paris-Sud, Paris-Saclay, Palaiseau, France

<sup>3</sup> Institute of Chemistry and Center of Interface Science, Carl von Ossietzky University, 26111 Oldenburg, Germany

<sup>4</sup> Max Planck Institute for Solid State Research, Heisenbergstraße 1, 70569 Stuttgart, Germany

<sup>5</sup> Institute for Experimental and Applied Physics, Christian Albrechts University in Kiel, Leibnizstr. 19, 24118 Kiel, Germany

<sup>6</sup> Forschungszentrum Neurosensorik, Carl von Ossietzky University, 26111 Oldenburg, Germany

\* christoph.lienau@uni-oldenburg.de

‡ These authors contributed equally

## 1. Simulation of the spectral interferometry algorithm

To validate the method of signal evaluation applied in Fig. 2 of the main text, we simulated the process of signal formation and retrieval based on an artificial input signal.

To obtain an artificial spectral interferogram, we first define a Gaussian excitation spectrum  $I_0(\omega)$  centered around  $\lambda_c=800$ nm (1.55 eV) with a FWHM of  $\Delta\omega=300$ meV as shown in Fig. S1a (dashed black). We furthermore define a nanorod spectrum  $\sigma(\omega)=|\sigma(\omega)|\,e^{i\varphi_\sigma(\omega)}$  via

$$\sigma(\omega)e^{i\omega\tau_0} = t_{21}\big(1+\beta^{(1)}\big) = t_{21}\cdot (1+iA_r\cdot L(\omega,\omega_0^r,\gamma^r)).$$

In the first order perturbation expression for  $\beta^{(1)} = M_{zz}(\omega, \mathbf{r}_t) - 1$  we have only retained a  $-\pi/2$  phase shift accounting for the resonant phase of  $\alpha_{zz}^t$ . For the lineshape function  $L(\omega, \omega_0^r, \gamma^r)$  of the rod LSP, we choose  $\hbar \omega_0^r = 1.51$  eV and  $\hbar \gamma^r = 0.037$  eV. To obtain a spectral interferogram that closely resembles the experimental data, we furthermore set  $\tau_0 = 100$  fs corresponding to a propagation distance of  $2L \approx 30$  µm,  $t_{21} = 0.1$  and  $A_r = 0.02$ . The propagators  $\overleftarrow{\mathbf{t}}_{sL}(\omega)$  and  $\overleftarrow{\mathbf{t}}_{ds}$  are set to unity.

Figure S1b shows the intensities of the Fourier transforms of  $S_+(\omega) = I_0(\omega)\sigma(\omega)$  (solid blue) and  $I_0(\omega)$  (dashed black).  $i_0(t)$  has a Fourier limited duration of  $\Delta t = \sqrt{4 \ln 2} / \Delta \omega = 7 \text{fs}$  and is centered around t = 0 whereas the time delayed field  $s_+(t - \tau_0)$  is centered around t = 100 fs. The time structure of  $s_+$  has acquired an asymmetric shape due to the free induction decay of the nanorod's LSP, which is clearly visible as an exponentially decaying tail at times t > 110 fs.

Figure S1c displays the spectral interferogram (SI) obtained by computing  $S(\omega) = I_0(\omega) |1 + \sigma(\omega)e^{i\omega\tau_0}|^2$ . In Fig. S1d, we show the Fourier transform  $s(t) = \mathcal{F}[S(\omega)]$  of this SI with contributions  $s_0(t)$  at t = 0 and  $s_+(t - \tau_0)$  at t = 100fs. Following the method described in the main text, we split these two components at the dashed vertical line and perform individual

Fourier back transforms. Panel e shows the two amplitude spectra  $S_0(\omega) = I_0(\omega)(1 + |\sigma(\omega)|^2)$  and  $S_+(\omega) = I_0(\omega)\sigma(\omega)$  with a pronounced absorptive dip at the energy of the LSP resonance. Finally, panel f displays the ratio  $S_+(\omega)/S_0(\omega)$  (solid red) and  $\varphi_{\sigma}(\omega) = \varphi_{S_+}(\omega)$  (dashed blue) which were calculated using Eqns. (5-6) from the methods section of the main text. The input amplitude and phase spectra from panel a are retrieved with good accuracy.

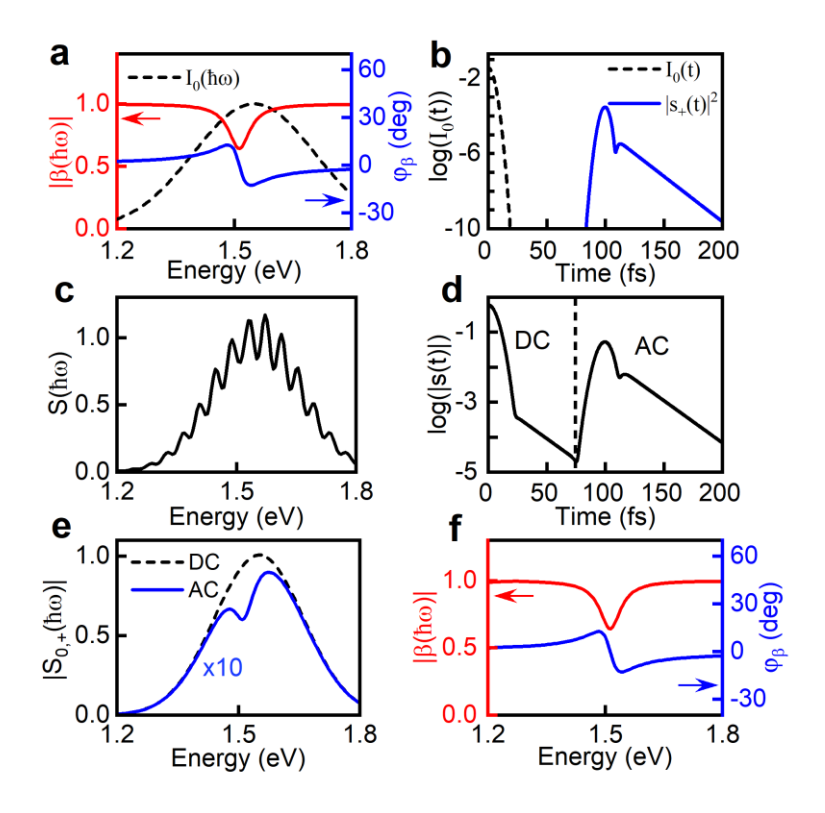


Figure S1. Simulation of spectral interferograms and scattering spectrum retrieval. a, Normalized Gaussian input laser spectrum (dashed black) together with the simulated absorptive Lorentzian resonance of the nanorod (solid red) and its phase (solid blue). b, Time-domain representation of the input pulse (dashed black), obtained by Fourier transformation of the laser spectrum. Time structure of  $|s_+|^2$  (solid blue), time delayed by  $\tau_0 = 100$  fs with respect to the incident pulse, after interaction with the LSP resonance of the nanorod in first perturbation order, i.e. for  $\beta^{(1)}(\omega) = 1 + M_{zz}(\omega, \mathbf{r}_t)$ . The free induction decay of the nanorod LSP resonance is visible at times t > 110 fs. c, Spectral interferogram  $S(\omega)$  between the incident field  $\mathbf{E}_1$  and the

back-reflected field  $\mathbf{E}_2$ .  $\mathbf{d}$ , Fourier transform of the interferogram in panel c with the DC contribution  $s_0(t)$  around t=0 and the positively delayed AC contribution  $s_+(t)$  around t=100 fs.  $\mathbf{e}$ , Separate inverse Fourier transforms of the DC (dashed black) and AC (solid blue) component in panel d. The AC component yields the modulated part of the spectrum.  $\mathbf{f}$ , Retrieved amplitude  $|\sigma(\omega)|$  (solid red) and phase spectrum  $\varphi_{\sigma}(\omega)$  (dotted blue) obtained using Eqns. (5) and (6) in the Methods. The input spectrum in panel (a) is fully reconstructed.

## 2. Coupled dipole simulation of the near-field interaction

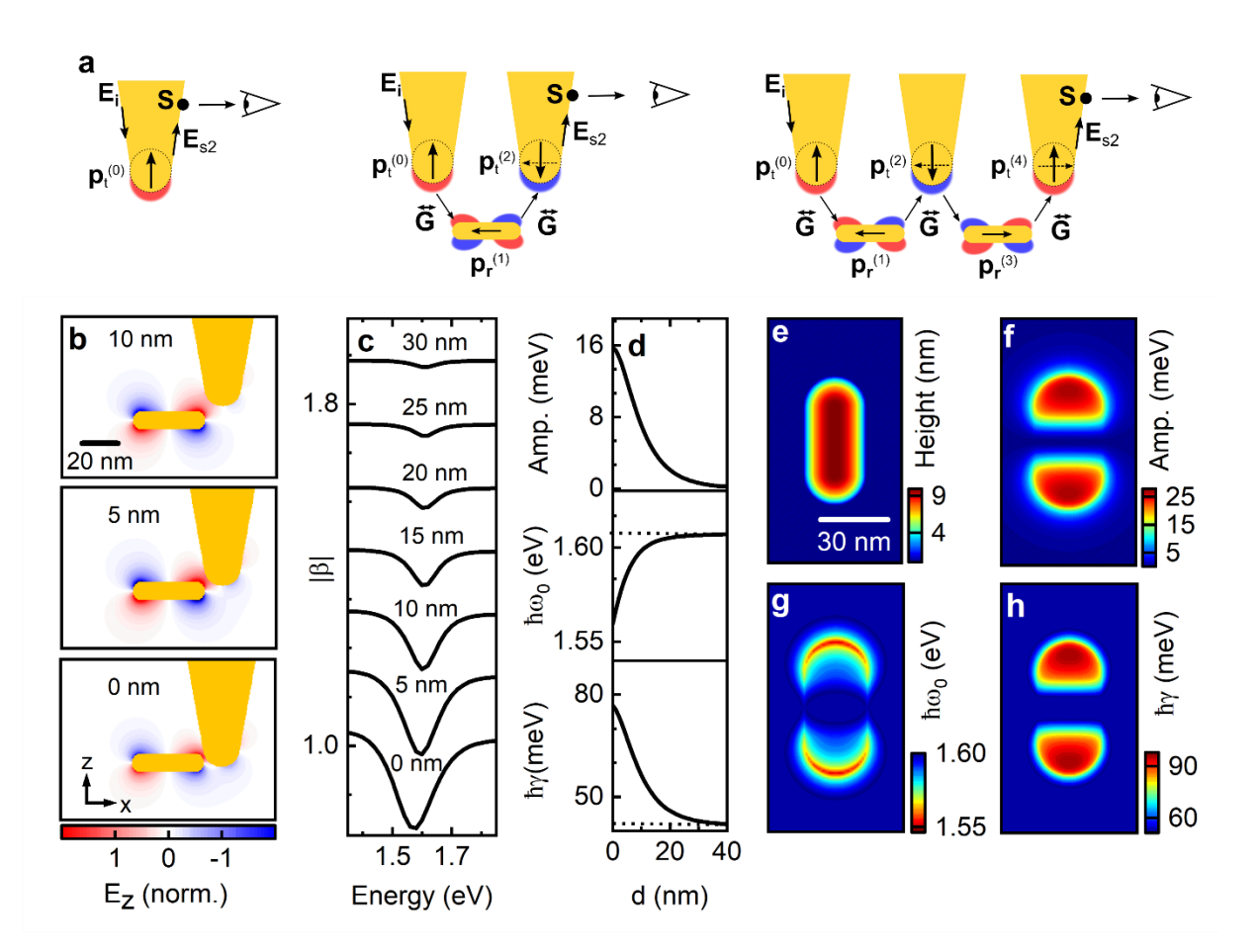


Figure S2. Coupled dipole analysis of PNSI spectra. a, Schematic representation of the zeroth, second and fourth perturbation order of the tip-nanorod interaction. In zeroth order, the incident SPP field  $\mathbf{E}_0(\omega, \mathbf{r}_t)$  induces a tip dipole moment  $\mathbf{p}_t^{(0)}$  along the tip axis. The z-component of  $\mathbf{p}_t^{(0)}$ 

excites a back-reflected SPP wave resulting in a field  $\mathbf{E}_{s2}(\omega, \mathbf{r}_s)$  at the position of a scatterer S on the taper shaft. This field interferes with the incident field  $\mathbf{E}_{s1}(\omega,\mathbf{r}_t)$  generating a far-field spectral interferogram. In the second and fourth order, tip-nanorod coupling leads to modifications of  $\mathbf{p}_{t}$ via the nanorod fields that couple back to the tip apex and induce dipole moments  $\mathbf{p}_t^{(2)}$  and  $\mathbf{p}_t^{(4)}$ . Since the tip resonance energy is very close to that of the rod,  $\mathbf{p}_t^{(2)}$  has a phase-shift of  $\pi/2$  relative to  $\mathbf{p}_r^{(1)}$  and hence a phase shift of  $\pi$  relative to  $\mathbf{p}_t^{(0)}$ . In second order, the nanorod scattering spectrum thus leads to absorptive signatures in the field  $\mathbf{E}_{s2}(\omega, \mathbf{r}_s)$  that is reconstructed from the spectral interferograms. b, Coupled dipole simulation of the near-field component  $E_z$  for three tipsample distances indicated in each panel. The calculation was performed assuming a spherical tip with a radius of 10 nm and a longitudinal LSP resonance energy of 1.61 eV for the nanorod. The line density  $\rho(x,x')$  of the nanorod polarizability was approximated by a chain of 11 polarizable point dipoles. Details of the simulations can be found in M. Esmann et al., Nature Nanotechnol. 14, 698 (2019). c, Simulated scattering spectra along a tip-sample approach curve. Tip-sample distances are indicated above each curve, subsequent curves are vertically offset for better visibility. To simulate the signature contained in the back-propagating SPP field  $\mathbf{E}_{s2}(\omega, \mathbf{r}_s)$ , we solely evaluate the far-field components emitted by the z-component of the resulting tip dipole moment  $p_{t,z}$  at a detection position 20  $\mu m$  away from the apex. At tip-sample distances below 20 nm, the spectra show a clear absorptive signature induced by the LSP resonance with increasing contrast as the tip-sample distance decreases. In this regime, the interaction-induced field enhancement  $\beta(\omega)$  provides a measure of the nanorod LDOS, since multiple reflections between tip and sample can be neglected. At distances below 10 nm both a pronounced red-shift and line broadening occur, which are the signatures of higher order tip sample coupling between the longitudinal LSP resonance of the nanorod and the transversal and longitudinal tip apex

polarizability, respectively. d, The line broadening and red-shift are quantified by fitting a Lorentzian lineshape to each spectrum of the approach curve. For tip-sample distances > 10 nm, the resonance parameters are approaching those of the unperturbed rod resonance indicated by black dotted lines. e, Simulated AFM topography of a single gold nanorod. f-h, Simulated Lorentzian parameter maps for a 2D scan, recorded by scanning the tip across the nanorod at close distance (0 nm) in (c). The amplitude map closely resembles the intensity profile of the zcomponent of the electric field of the LSP mode of the nanorod,  $|\mathbf{e}_{LSP}(\mathbf{r}_t) \cdot \mathbf{e}_z|^2$ . While the coupling induced red-shift is mainly concentrated in two crescent-moon-shaped lobes at the nanorod apices, the spectral line broadening correlates with maps of the mode profile of the LSP mode, i.e, it provides a measure for the projected local density of states of the nanorod. The difference between the maps in panels g and h highlights the vectorial nature of tip-sample interaction mediated by the longitudinal and transversal tip polarizability components. The simulation demonstrates that for a reconstruction of the nanorod LDOS a tip-sample distance of roughly > 8 nm should be maintained. Below this value, multiple tip-sample scattering takes place leading to rich coupling effects.

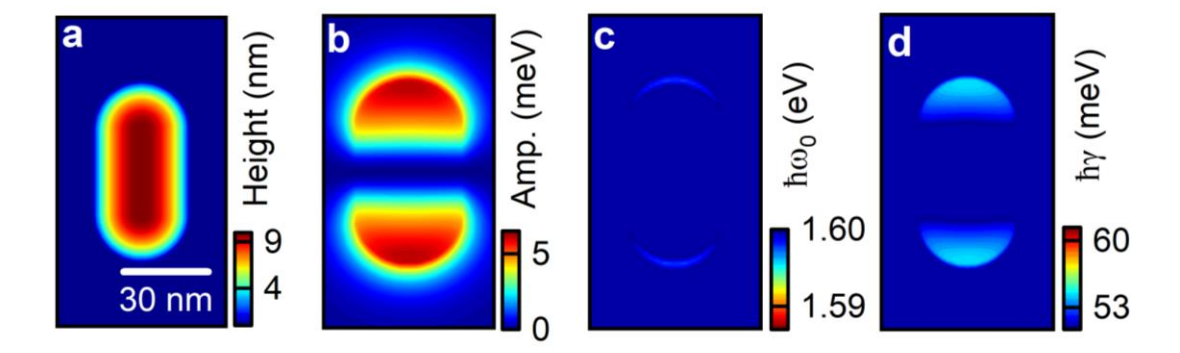


Figure S3. Coupled dipole analysis of PNSI spectra at increased tip-sample distance of 8 nm. The coupled dipole simulations are performed using the same tip and nanorod properties as chosen for the simulations in Fig. S2, except for the tip-sample distance which is increased by 8 nm. (a)

Topography, (b) amplitude of the PNSI signal, (c) resonance energy shift, (d) coupling-induced line broadening. The increase in tip-sample distance reduces the amplitude of the PNSI signal by a factor of 4 with respect to that in Fig. S2 (f). At the same time, the resonance energy shifts and line broadenings observed in Fig. S2 have almost vanished. This allows for a faithful imaging of the nanoparticle LDOS with a spatial resolution of better than 10 nm.